



Daily Drought Prediction in the Huaihe River Basin Using VMD-informer-LSTM

Min Li, Ming Ou, Yuhang Yao, Changman Yin

College of Hydraulic Science and Engineering, Yangzhou University, Yangzhou, China, 225000

Correspondence to: Min Li (limitju@126.com)

Abstract

Accurate drought prediction is a key challenge in water resource management and agricultural planning. This study proposes a novel drought prediction framework that integrates Variational Mode Decomposition (VMD), Informer, and Long Short-Term Memory (LSTM) networks to enhance hydrological drought forecasting in the Huaihe River Basin, China. The VMD-Informer-LSTM model decomposes complex non-stationary drought sequences into multi-scale components, effectively extracting long-term trends and short-term fluctuations. Results show that the model outperforms LSTM, Transformer-LSTM, and Informer-LSTM, improving R^2 , RMSE, MAE, and MAPE by 28.4%, 46.2%, 46.5%, and 50.8%, respectively, over the baseline LSTM. When the prediction period is 30 days, the VMD-Informer-LSTM achieves the highest prediction accuracy. During the 120–180 day prediction period, the prediction accuracy of all models declines, with drought intensity generally underestimated. Misclassifications are mainly concentrated in the transition zones between humid and semi-humid regions, with higher error frequency in semi-humid areas. Prediction accuracy is highest in the upstream and downstream regions, followed by the Yishuisi River Basin, while the midstream region performs poorly due to human interference. Shapley Additive Explanations (SHAP) further reveal that precipitation and temperature are the dominant meteorological drivers, jointly accounting for nearly half of the model's predictive power. These results confirm that the VMD-Informer-LSTM provides the most accurate predictions among the tested models, offering valuable support for drought risk assessment and water resource management in the Huaihe River Basin and other similar regions.

Keywords: Drought prediction, DEDI, Variational Mode Decomposition, informer, LSTM

1 Introduction

Drought represents one of the most spatially extensive, temporally persistent, and far-reaching natural disasters globally, with complex formation mechanisms involving intricate interactions between atmospheric circulation patterns, land surface processes, and human activities (Alsubih et al., 2021; Dai, 2013). Drought events not only directly threaten watershed water security and agricultural productivity but also profoundly affect regional ecosystem stability and socioeconomic development (Zhang et al., 2018). With intensifying climate change and increasing human activity intensity, drought events exhibit significant upward trends in frequency, intensity, and spatial extent (Cook et al., 2020; Trenberth et al., 2014). Therefore, accurate drought prediction is crucial for developing scientific disaster mitigation strategies, optimizing water resource allocation schemes, and ensuring regional food and ecological security.

However, drought prediction faces major challenges due to the inherent complexity of drought



phenomena (Hao et al., 2017). Drought occurrence and evolution are controlled by multiple natural and anthropogenic factors, including precipitation distribution, evapotranspiration processes, topographic conditions, land use changes, and human interventions (AghaKouchak et al., 2015; Vicente-Serrano et al., 2018). These factors generate highly complex, nonlinear, and non-stationary spatiotemporal evolution patterns. Drought time series typically contain multi-scale periodic oscillations, long-term trend changes, and stochastic fluctuation components that are mutually coupled and interdependent, forming extremely complex dynamical systems (Belayneh et al., 2014; Huang et al., 2015).

Traditional drought prediction methods rely on physics-based numerical models and statistical regression approaches (Dutra et al., 2014; Yuan & Quiring, 2017). Physics-based methods include Global Climate Models (GCMs) such as the ECMWF and NCEP-CFSv2, which can provide global-scale long-term climate predictions but have coarse spatial resolutions (typically 100-200 km) and cannot adequately capture regional drought characteristics (Saha et al., 2014). Regional Climate Models (RCMs) employ dynamic downscaling techniques to achieve high resolutions (10-50 km) but inherit systematic biases from driving models and require substantial computational resources (Jacob et al., 2014; Rummukainen, 2010). Land surface models such as Variable Infiltration Capacity (VIC), Community Land Model (CLM), and Noah simulate coupled water cycle, energy balance, and vegetation dynamics processes but are highly sensitive to meteorological forcing data quality and parameterization schemes (Ek et al., 2003; Lawrence et al., 2011). Statistical methods include linear regression approaches, time series analysis and spectral/wavelet analysis techniques, etc (Box et al., 2015; Modarres, 2007). Time series models, such as Autoregressive Moving Average (ARMA), Autoregressive Integrated Moving Average (ARIMA) models, Random Forest (RF), demonstrate certain capabilities for stationary time series. However, their prediction performance significantly deteriorates on non-stationary, multi-periodic drought sequences (Mishra & Desai, 2005; Mossad & Alazba, 2015). Despite contributions from these traditional methods, fundamental limitations persist across both physics-based and statistical approaches (Hao et al., 2017; Morid et al., 2006). Rigid model structures in both GCMs and RCMs cannot adaptively adjust to accommodate intrinsic data characteristics. Insufficient nonlinear processing capabilities in land surface models and statistical methods (including ARMA, ARIMA, and RF models) cannot capture complex feedback mechanisms and threshold effects (AghaKouchak et al., 2015). Additionally, there are difficulties in multi-scale information integration and heterogeneous data fusion, particularly in land surface models and GCMs (Wood et al., 2016). High parameter sensitivity affects the robustness and generalization capability of both physics-based and statistical models (including ARMA, ARIMA, and RF models) (Svoboda et al., 2002). Finally, trade-offs between computational efficiency and accuracy challenge the operational implementation requirements of RCMs and complex statistical models (Mo, 2008; Yuan & Quiring, 2017).

Recent advances in artificial intelligence and big data technologies have fundamentally transformed time series modeling and prediction across multiple fields (LeCun et al., 2015; Shlezinger et al., 2023). Deep learning methods demonstrate significant advantages in automatically capturing complex patterns and latent features without requiring pre-specified physical relationships, possessing powerful nonlinear mapping and adaptive learning capabilities (Bengio et al., 2013; Schmidhuber, 2015). Long-Short-Term Memory (LSTM) networks have been successfully applied



83 to various hydrological nonlinear sequence modeling tasks, including streamflow prediction, flood
 84 forecasting, and water level estimation, demonstrating superior predictive performance (Kratzert et
 85 al., 2018; Zhang et al., 2014). LSTM networks through their unique gate mechanisms and memory
 86 cell design effectively address gradient vanishing problems in traditional recurrent neural networks
 87 and exhibit excellent performance in capturing long-term dependency information (Greff et al.,
 88 2017). However, single deep learning architectures still have limitations when processing complex
 89 time series data, and multi-model ensemble and parallel architecture designs provide novel
 90 approaches for further enhancing prediction performance (Mosavi et al., 2018; Sit et al., 2020).

91 To enhance model capability for processing non-stationary complex sequences, signal
 92 decomposition algorithms for data preprocessing have become key strategies for improving time
 93 series prediction performance. Variational Mode Decomposition (VMD), an advanced adaptive
 94 signal decomposition technique proposed by Dragomiretskiy and Zosso in 2014, decomposes non-
 95 linear, non-stationary complex sequences into multiple Intrinsic Mode Functions (IMFs) with
 96 different center frequencies. Each IMF reflects the dynamic characteristics of the original sequence
 97 at specific frequency levels, possessing relatively independent frequency bandwidth and amplitude
 98 modulation properties (Dragomiretskiy & Zosso, 2014). Compared to traditional decomposition
 99 methods such as Empirical Mode Decomposition (EMD) and Ensemble EMD (EEMD), VMD is
 100 based on rigorous variational optimization theoretical frameworks, employs completely non-
 101 recursive decomposition models, effectively avoids mode mixing and end-effect problems, and
 102 possesses superior frequency separation effects and noise robustness.

103 In recent years, Transformer architectures have achieved major breakthroughs in time series
 104 prediction, particularly the informer model specifically optimized for long time series prediction
 105 tasks. Zhou proposed that informer reduces computational complexity from $O(L^2)$ to $O(L \log L)$
 106 through Probabilistic Sparse Self-attention mechanisms, combined with self-attention distillation
 107 operations that progressively compress sequence length layer by layer, significantly improving
 108 efficiency and accuracy in processing lengthy sequences (Zhou et al., 2021a). This innovative
 109 architecture provides novel technical pathways for capturing long-range temporal dependencies.

110 This study adopts the Daily Evapotranspiration Deficit Index (DEDI) as a drought monitoring
 111 indicator, constructed based on daily actual and potential evapotranspiration from ERA5 reanalysis
 112 data, which can effectively reflect the dynamic evolution processes of regional droughts (Hersbach
 113 et al., 2020; Zhang et al., 2022; Zuo et al., 2020). Building upon this foundation, we propose a novel
 114 drought prediction model integrating Variational Mode Decomposition, informer, and Long Short-
 115 Term Memory networks (VMD-informer-LSTM), which is expected to provide a high-accuracy,
 116 robust prediction framework for drought prediction applications by combining the technical
 117 advantages of variational optimization decomposition, probabilistic sparse attention mechanisms,
 118 and gated memory networks. Through a combination of multiscale feature decomposition and
 119 hybrid deep learning architectures, this method effectively handles the non-stationary characteristics
 120 of complex drought indices like DEDI, accurately capturing long-range climate trends and short-
 121 term fluctuations. This study significantly improved prediction accuracy and reliability of complex
 122 non-stationary drought time series and provided scientific foundations for regional water resource
 123 management and drought risk assessment (Pozzi et al., 2013; Willmott & Matsuura, 2005).

124 The technical approach includes: (1) utilizing VMD for adaptive modal decomposition of
 125 original DEDI sequences, deconstructing complex nonlinear time series into multi-frequency scale
 126 IMF components to achieve structured extraction of multi-scale features (Dragomiretskiy & Zosso,



2014; Johny et al., 2022); (2) constructing dual-branch parallel architecture of informer and LSTM, where informer efficiently captures global trends of long-range sequences through probabilistic sparse attention mechanisms, while LSTM precisely models local temporal dynamics through gating mechanisms (Zhou et al., 2021b); (3) fusing dual-source features through fully connected layers to form hybrid feature representations possessing both long-range dependency analysis capability and short-term fluctuation capture ability (Li et al., 2023; Zhang et al., 2019); (4) adopting a three-stage design of decomposition-parallelization-fusion to obtain final drought prediction results.

2 Study Area and data

2.1 Study Area

The Huaihe River Basin originates from the Tongbai Mountains in Nanyang City, Henan Province, China. It is located between 111°55'-121°20'E longitude and 30°55'-36°20'N latitude, covering approximately 270,000 km². The basin is situated in China's north-south climate transition zone, with the area north of the Huaihe River belonging to the warm temperate zone and the area south of the river belonging to the northern subtropical zone (Yao et al., 2024). The annual mean temperature ranges from 11-16°C, with temperature variations increasing from north to south and from coastal to inland areas. The Huaihe River Basin receives a multi-year average precipitation of 883 mm, with a spatial distribution characterized by higher precipitation in mountainous areas compared to plains, increased precipitation along the coast than inland, and a decreasing gradient from south to north. The multi-year average evaporation in the basin fluctuates between 650-1250 mm, primarily concentrated during May-August, with an overall decreasing trend from south to north and from east to west. The studied region is shown in Fig. 1.

During the 62-year period from 1949 to 2010, the Huaihe River Basin experienced cumulative drought-affected areas of 167 million hectares, with disaster-affected areas of 87.3 million hectares, resulting in grain losses of 13.96 billion kg. On average, 2.698 million hectares of crops were affected by drought annually, with 1.408 million hectares suffering disaster-level impacts (Gao et al., 2015). Drought disasters have severely impacted industrial and agricultural production, urban and rural water supply security, and ecological environments within the basin, becoming one of the primary factors constraining rapid and sustainable socio-economic development in the region. Therefore, providing reliable drought prediction methods is of great significance for accurate drought forecasting and the scientific development of drought response strategies in the Huaihe River Basin.

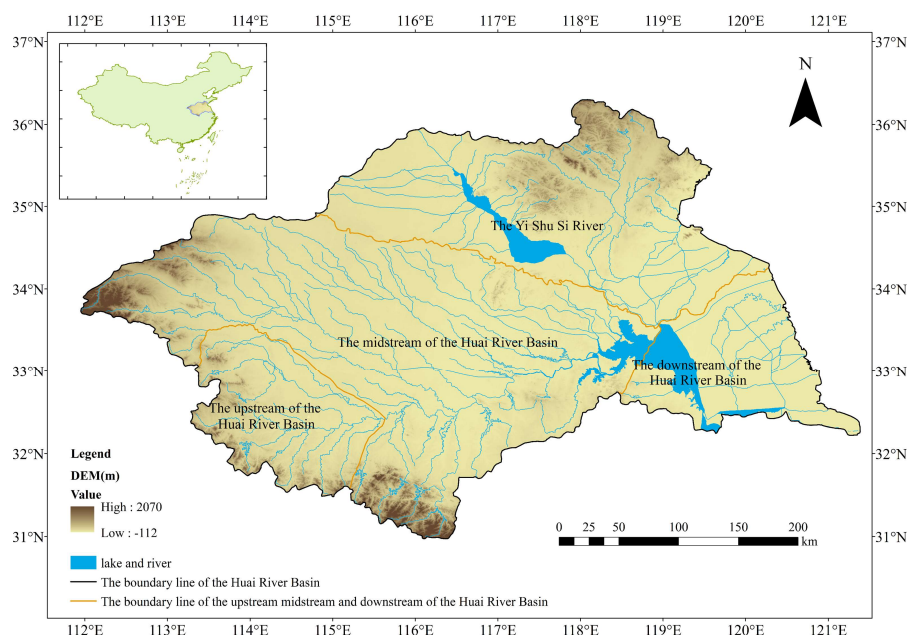


Figure 1 The study area of Huaihe river Basin

2.2 Data Sources

This study utilizes daily actual evapotranspiration, potential evapotranspiration, surface pressure, cloud cover, maximum temperature, mean temperature, wind speed, and precipitation data for the period 1980-2020, sourced from the fifth-generation high-resolution atmospheric reanalysis product (ECMWF Reanalysis v5, ERA5) developed by the European Centre for Medium-Range Weather Forecasts (ECMWF). ERA5 data are characterized by extensive coverage, long time series, and excellent spatio-temporal consistency. This makes them an optimal data choice for long-term and high-resolution analyses. To meet the specific spatial resolution requirements of this study, the downloaded ERA5 data were further subjected to interpolation processing. This converted them to a spatial resolution of $0.25^\circ \times 0.25^\circ$ to more precisely match the spatial characteristics of the study region (Muñoz-Sabater et al., 2021). Land use data for 2005, 2010, 2015, and 2020 with a spatial resolution of 1 km were obtained from the Data Center for Resources and Environmental Sciences, Chinese Academy of Sciences (<https://www.resdc.cn/>).

3. Methods

3.1 DEDI Index

The Daily Evapotranspiration Deficit Index (DEDI) is a daily drought index constructed based on daily evapotranspiration as well as potential evapotranspiration for monitoring and predicting regional drought events (Zhang et al., 2022). This index is calculated based on ERA5 data provided by ECMWF.

The DEDI is calculated as follows:



$$DEDI_i = \frac{D_i - D_{AVE}}{D_{STU}} \quad (1)$$

$$D_i = AET_i - PET_i \quad (2)$$

where i represents time, AET_i represents the actual evapotranspiration on day i (units: mm/day), PET_i represents the potential evapotranspiration on day i (units: mm/day), D_i represents the evapotranspiration deficit between AET and PET on day i , and D_{AVE} and D_{STU} are the multi-year climatological mean and standard deviation, respectively (Zuo et al., 2020).

3.2 VMD

Variational Mode Decomposition (VMD) was proposed by Konstantin Dragomiretskiy (Dragomiretskiy & Zosso, 2014) as a signal processing method designed to effectively overcome mode mixing and end effect problems existing in Empirical Mode Decomposition (EMD). Unlike the recursive decomposition principle of EMD, VMD determines the central frequency and bandwidth of each mode component. This is done by constructing and solving the optimal solution to a variational model. This represents a completely non-recursive decomposition model. This method searches for a set of mode components and their corresponding center frequencies through an iterative search. This ensures that each mode maintains smoothness after demodulation to baseband.

The adaptivity of VMD is reflected in its ability to automatically determine the number of modes decompositions according to signal characteristics and adaptably match the optimal center frequency and finite bandwidth for each mode, thereby achieving effective separation of Intrinsic Mode Functions (IMFs) and frequency domain partitioning of signals. Experimental results demonstrate that VMD exhibits strong robustness in sampling and noise aspects, is capable of reducing the non-stationarity of time series with high complexity and strong non-linearity and decomposing them into multiple sub-sequences with different frequency scales that are relatively stationary, making it particularly suitable for non-stationary signal processing.

VMD decomposes time series into simple high-frequency and low-frequency intrinsic mode functions through optimization processes, improving signal processing stability and accuracy. This method is not only theoretically innovative but also demonstrates superior performance in practical applications, providing an effective tool for non-stationary signal analysis. Research by Zhao et al. (2023) further proved VMD's excellent performance in handling boundary effects by adjusting parameters (such as decomposition levels, quadratic penalty terms, etc.) to effectively control deviations in decomposition results, thereby improving model adaptability (Zhang et al., 2023; Zhao et al., 2023).

Assuming the original signal f is decomposed into k components, ensuring that the decomposed sequences are modal components with finite bandwidth and center frequencies, while minimizing the sum of estimated bandwidths of all modes, with the constraint that the sum of all modes equals the original signal, the VMD constrained variational model is as follows:

$$\min_{\{u_k, \omega_k\}} \left\{ \sum_{k=1}^K \left\| \partial_t \left[\left(\delta(t) + \frac{j}{\pi t} \right) * u_k(t) \right] e^{-j\omega_k t} \right\|_2^2 \right\} \quad (3)$$

$$\text{s.t. } \sum_k u_k = f(t) \quad (4)$$

$$u_k = \{u_1, u_2, \dots, u_k\} \quad (5)$$



$$\omega_k = \{\omega_1, \omega_2, \dots, \omega_k\} \quad (6)$$

where $f(t)$ represents the original data; K represents the number of modal components; $\delta(t)$ represents the Dirac function; $*$ represents convolution operation; ∂_t is the partial derivative operator; $\{u_k\}$ represents the k -th component function obtained through calculation; $\{\omega_k\}$ represents the center frequency of the k -th component obtained through calculation.

The augmented LaGrange is introduced to solve this constrained optimization problem:

$$L(\{u_k\}, \{\omega_k\}, \lambda) = \alpha \sum_k \left\| \partial_t \left[\left(\delta(t) + \frac{j}{\pi t} \right) * u_k(t) \right] e^{-j\omega_k t} \right\|_2^2 + \left\| f(t) - \sum_k u_k(t) \right\|_2^2 + \left(\lambda(t), f(t) - \sum_k u_k(t) \right) \quad (7)$$

where α represents the penalty factor; $\lambda(t)$ represents the Lagrange multiplier.

The alternating direction method of multipliers (ADMM) is used to find the saddle point of the augmented LaGrange. In the frequency domain, the updates are:

$$\hat{u}_k^{n+1}(\omega) = \frac{\hat{f}(\omega) - \sum_{i \neq k} \hat{u}_i^{n+1}(\omega) + \frac{\hat{\lambda}^n(\omega)}{2}}{1 + 2\alpha(\omega - \omega_k^n)^2} \quad (8)$$

$$\omega_k^{n+1} = \frac{\int_0^\infty \omega |u_k^{n+1}(\omega)| d\omega}{\int_0^\infty |u_k^{n+1}(\omega)| d\omega} \quad (9)$$

$$\hat{\lambda}^{n+1}(\omega) \leftarrow \hat{\lambda}^n(\omega) + \pi \left[\hat{f}(\omega) - \sum_{i \neq k} \hat{u}_i^{n+1}(\omega) \right] \quad (10)$$

where γ represents noise tolerance; the $\hat{u}_k^{n+1}(\omega)$ represent Wiener filtering residuals; $\hat{u}_i(\omega)$ and $\hat{\lambda}^n(\omega)$ represent the Fourier transforms of $u(t)$ and $\lambda(t)$, respectively.

3.3 LSTM

The Long-Short-Term Memory (LSTM) models are a special type of Recurrent Neural Network (RNN) variant that addresses the gradient vanishing problem in RNN processing of long sequence data by introducing memory cells (Cell States), specifically designed for processing time series data (Hochreiter & Schmidhuber, 1997). When recording long sequence data, RNN experiences gradient vanishing or exploding due to continuous information accumulation, making it difficult for the network to learn long-term dependencies, ultimately affecting the model's accurate capture of trends and periodicity in time series data (Jaseena & Koor, 2022).

LSTM aims to solve the gradient-vanishing or exploding problems encountered by traditional RNN when processing long sequence data. This is done mainly through gate mechanisms regulating information flow. The LSTM model consists of four interacting layers: input gate, forget gate, cell state gate, and output gate. It is shown in Fig. 2 below.

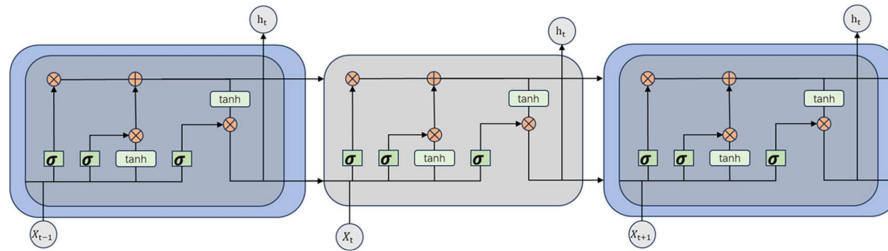


Figure 2 The construction of LSTM

3.4 informer

informer is an improved and optimized version based on Transformer, specifically designed to enhance the speed and efficiency of processing long sequences and optimized for long-term time series prediction tasks (Zhou et al., 2021b). Transformer captures relationships between different positions in sequences through Self-Attention mechanisms. However, Transformer encounters difficulties when processing long time series data because its computational complexity grows quadratically with sequence length, becoming very slow or even unprocessable when dealing with very long time series.

informer proposes ProbSparse Self-attention to filter critical queries and reduce computational complexity, and introduces Self-attention Distilling to reduce dimensions and network parameters (Vaswani et al., 2017). As shown in Fig. 3, the informer architecture consists of an encoder-decoder structure. Input sequences first undergo convolutional encoding and positional embedding before being fed into the encoder; the encoder utilizes multi-layer probabilistic sparse self-attention and distillation operations to extract key information, outputting encoded features. The decoder then directly generates long sequence predictions under masked self-attention and cross-attention, followed by fully connected layers mapping to final values.

For long sequence prediction, the informer has three advantages: 1. Probabilistic sparse self-attention reduces time complexity from $O(L^2)$ to $O(L \log L)$, significantly reducing computational overhead; 2. Self-attention distillation progressively compresses the sequence length layer by layer, simultaneously reducing computation and memory requirements; 3. Generative decoding outputs complete future sequences at once, avoiding error accumulation caused by step-by-step extrapolation.

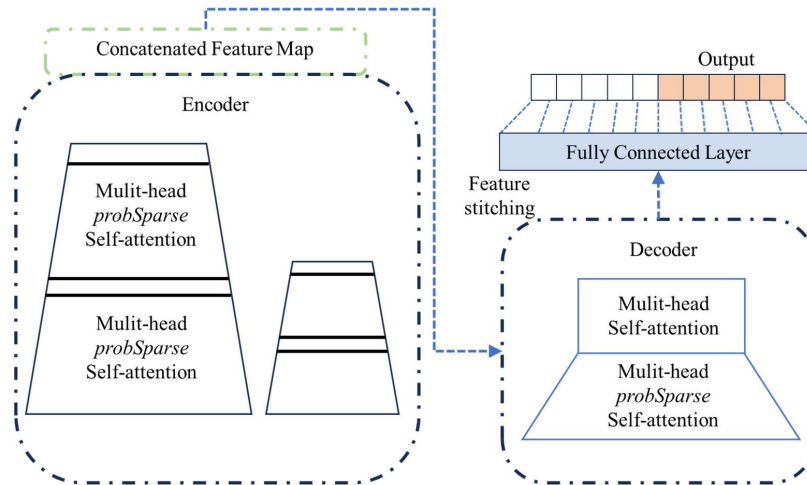


Figure 3 The construction of the informer

3.5 VMD-informer-LSTM

The VMD-informer-LSTM model employs Variational Mode Decomposition (VMD) to deconstruct DEDI time series into multi-frequency scale Intrinsic Mode Functions (IMFs), achieving the structured extraction of multi-scale features. Based on this foundation, it constructs a dual-branch parallel architecture of informer and LSTM, where informer efficiently captures global trends of long-range sequences through probabilistic sparse attention mechanisms, while LSTM precisely models local temporal dynamics through gate mechanisms. Finally, dual-source features are fused through fully connected layers to form hybrid feature representations possessing both long-range dependency analysis capability and short-term fluctuation capture ability. This model significantly improves prediction accuracy and reliability for complex time series data through a three-stage design of decomposition-parallelization-fusion, providing an innovative solution for time series prediction tasks. The construction of VMD-informer-LSTM is shown in Fig. 4 below.

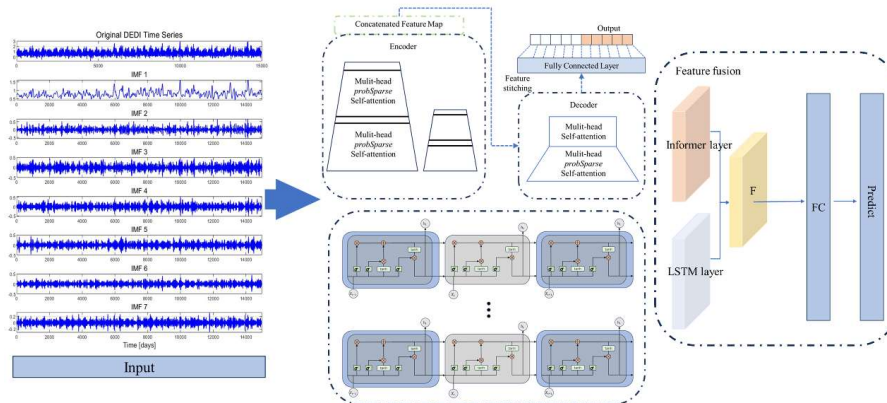


Figure 4 The construction of VMD-informer-LSTM



3.5 Shapley Additive Explanations

Since machine learning models are “black-box” models, although they can provide efficient predictions, their internal decision-making processes are complex and difficult to intuitively understand and explain. This may affect result analyses in the field of raster data, which require transparency and interpretability. To overcome such problems, SHAP values are introduced as an interpretive method. The SHAP value method was proposed by Lundberg et al (Lundberg & Lee, 2017). In 2017, it is a method based on cooperative game theory that quantifies the contribution of driving factors to model prediction results. By calculating the marginal contributions of each factor to the model output under different combinations, it measures their importance in the overall prediction results. This helps us understand how the model makes decisions. The positive or negative values of SHAP indicate promotion or inhibition of prediction results. The absolute value reflects the degree of influence of the factor on the model prediction results. The larger the absolute value, the greater the influence of the factor on model prediction results (Wang et al., 2024). The formula is as follows:

$$\phi_i = \sum_{S \in N \setminus \{i\}} \frac{|S|! (|N| - |S| - 1)!}{|N|!} [f(S \cup \{i\}) - f(S)] \quad (11)$$

In the formula, ϕ_i represents the SHAP value for feature i ; N is the set of all features; S is a subset of features, excluding feature i ; $f(S)$ is the model output using only the feature subset S for prediction; $f(S \cup \{i\})$ is the predicted value after adding feature i to the featured subset S .

3.6 Evaluation Metrics

The coefficient of determination (R^2) measures the proportion of variance in the dependent variable that is derived from the independent variable, ranging from 0 to 1, where values closer to 1 indicate better model performance (Nash & Sutcliffe, 1970). The root mean square error (RMSE) quantifies the average magnitude of prediction errors, providing a measure of how well the model predicts actual values, with lower values indicating better accuracy (Willmott & Matsuura, 2005). Mean absolute error (MAE) represents the average absolute difference between predicted and observed values, offering a linear score that is less sensitive to outliers than RMSE. The range of mean absolute percentage error (MAPE) is $[0, +\infty]$. A MAPE of 0% indicates a perfect model, while a MAPE greater than 100% suggests a poor model (Myttenaere et al., 2016).

The mathematical expressions for these metrics appear as follows:

$$R^2 = 1 - \frac{SSE}{SST} = 1 - \frac{\sum_{i=1}^N (y_{obs} - y_{pred})^2}{\sum_{i=1}^N \Sigma (y_{obs} - \bar{y}_{obs})^2} \quad (12)$$

$$RMSE = \sqrt{\frac{1}{N} \sum_{i=1}^N (y_{obs} - y_{pred})^2} \quad (13)$$

$$MAE = \frac{1}{N} \sum_{i=1}^N |y_{obs} - y_{pred}| \quad (14)$$



$$MAPE = \frac{1}{N} \sum_{i=1}^N \text{abs} \left(\frac{y_{obs} - y_{pred}}{y_{obs}} \right) \quad (15)$$

where y_{obs} represents observed values, y_{pred} represents predicted values, \bar{y}_{obs} is the mean of observed values, and n is the number of observations.

4. Results and Discussion

4.1 VMD Decomposition Results

In this study, we systematically selected 108 grid points distributed across the Huaihe River Basin and performed VMD analysis of their corresponding daily DEDI time series data spanning 1980-2020. Fig. 5 provides a comprehensive visual representation of the decomposed sub-sequences of DEDI data for a certain representative grid cell in the Huaihe River Basin. As illustrated in Fig. 5, the daily DEDI values for a representative grid cell in the Huaihe River Basin exhibit substantial positive and negative fluctuations, with considerable variance between maximum and minimum values. These pronounced oscillations present significant challenges in capturing essential features during the prediction process, as the complex, non-stationary nature of the original signal obscures the underlying patterns and trends. The VMD algorithm successfully decomposes the complex, non-linear DEDI time series into multiple distinct IMFs, each characterized by specific frequency bands and temporal scales. These decomposed components reveal multi-scale variability patterns ranging from high-frequency short-term fluctuations to low-frequency long-term trends, facilitating more effective feature extraction and modeling processes. VMD technology demonstrates superior capability in accurately tracking changes in signal frequency components and effectively revealing the intrinsic and dynamic characteristics of time series, thereby substantially enhancing prediction accuracy and reliability.

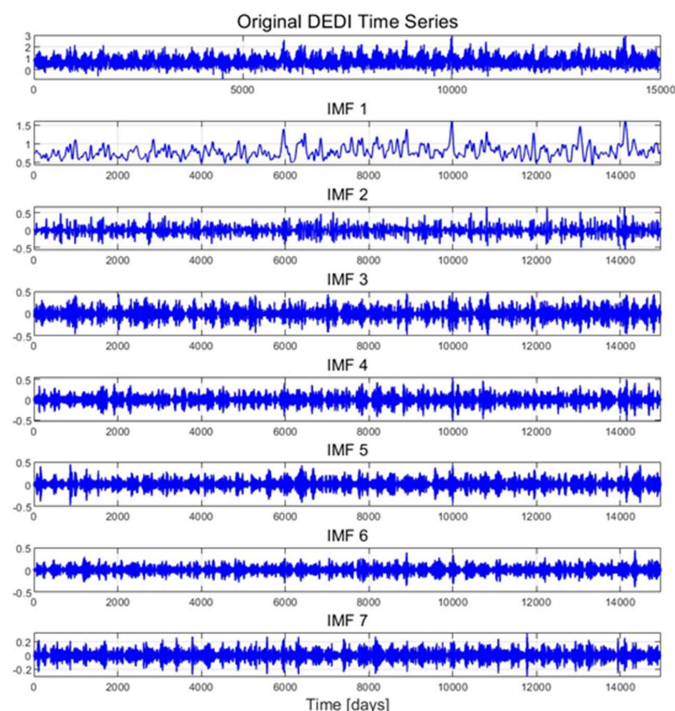


Figure 5 The daily DEDI values of a certain grid in the Huaihe River Basin are decomposed into 7 sub - sequence through variational mode decomposition (VMD).

4.2. Model Prediction Performance Evaluation

To evaluate the performance of the proposed VMD-informer-LSTM model, we performed extensive comparative experiments involving four distinct modeling approaches: the proposed VMD-informer-LSTM model, the informer-LSTM model, the Transformer-LSTM model, and the standalone LSTM model. The evaluation of each model's performance was based on four widely used statistical metrics for time series prediction evaluation. From Table 1, it can be seen that the VMD-informer-LSTM model performs the best in terms of predictive performance, with R^2 , RMSE, MAE, and MAPE reaching 0.9191, 0.1122, 0.0778, and 0.4056, respectively. In contrast, the informer-LSTM model without VMD decomposition has R^2 , RMSE, MAE, and MAPE of 0.8570, 0.1498, 0.1031, and 0.5330, respectively. After calculation, VMD decomposition improves R^2 , RMSE, MAE, and MAPE by 7.25%, 25.10%, 24.54%, and 23.90%, respectively. Furthermore, the traditional LSTM model shows relatively low predictive accuracy with four evaluation metrics of $R^2=0.7156$, RMSE=0.2087, MAE=0.1454, and MAPE =0.8254. The Transformer-LSTM model achieves R^2 , RMSE, MAE, and MAPE of 0.8286, 0.1641, 0.1130, and 0.6266, respectively. This, although better than the basic LSTM model, is still not as good as the informer-LSTM model, let alone the VMD-informer-LSTM model. In summary, by comparing the predictive performance of the four models, it is evident that the VMD-informer-LSTM model has an advantage in time series prediction tasks. Especially after the introduction of VMD decomposition, its performance has



significantly improved, further verifying the effectiveness of VMD decomposition in enhancing model predictive accuracy.

Table 1 Overall average evaluation indicators of various models within the Huaihe River Basin

Indicator	LSTM	Transformer-LSTM	informer-LSTM	VMD-informer-LSTM
R ²	0.7156	0.8286	0.8570	0.9191
RMSE	0.2087	0.1641	0.1498	0.1122
MAE	0.1454	0.1130	0.1031	0.0778
MAPE	0.8254	0.6266	0.5330	0.4056

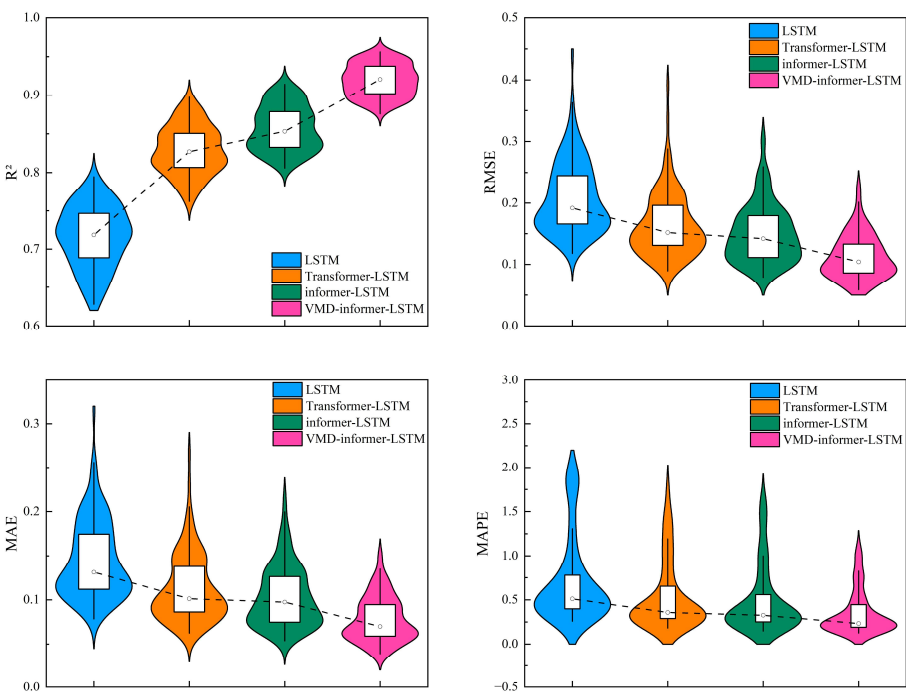


Figure 6 Violin-box plots of evaluation indicators for different models in the Huaihe River Basin

Fig. 6 presents violin plots illustrating the distribution of evaluation metrics across all 108 grid points in the Huaihe River Basin. This provides insights into model performance variability and consistency. Violin plots reveal important patterns. The VMD-informer-LSTM model demonstrates the most concentrated distribution around optimal values, with R² distributions tightly clustered near 0.92-0.95, indicating consistent and high performance across diverse geographical locations. Error metric distributions (RMSE, MAE and MAPE) show the VMD-informer-LSTM model has the narrowest spread and the lowest median values, suggesting robust prediction accuracy with minimal spatial variability.

The RMSE distributions demonstrate a clear monotonic improvement from LSTM (median: 0.2087) through Transformer-LSTM (0.1641), informer-LSTM (0.1498) to VMD-informer-LSTM (0.1122), with progressively narrower interquartile ranges and fewer outliers. The VMD-informer-



366 LSTM model exhibits the most concentrated distribution with minimal dispersion (IQR: 0.05),
367 indicating superior prediction accuracy and enhanced stability across diverse geographical locations.
368 This concentrated performance distribution reflects the effectiveness of combining VMD
369 decomposition with hybrid deep learning architectures for robust drought prediction.

370 Comparing the four models, the VMD-informer-LSTM model consistently outperforms the
371 other three, with an average R^2 of 0.9191, RMSE of 0.1122, MAE of 0.0778, and MAPE of 0.4056.
372 The informer-LSTM model without VMD decomposition has an average R^2 of 0.8570, RMSE of
373 0.1498, MAE of 0.1031, and MAPE of 0.5330. The Transformer-LSTM model achieves an average
374 R^2 of 0.8286, RMSE of 0.1641, MAE of 0.1130, and MAPE of 0.6266. The basic LSTM model has
375 the lowest performance, with an average R^2 of 0.7156, RMSE of 0.2087, MAE of 0.1454, and
376 MAPE of 0.8254.

377 The performance improvement from LSTM to Transformer-LSTM to informer-LSTM is
378 evident, with each model showing better median values and reduced spread in the error metrics
379 compared to the previous one. However, the VMD-informer-LSTM model stands out with the most
380 significant enhancements in both median performance and reduced variance across all metrics. This
381 indicates that the integration of VMD decomposition with the informer-LSTM architecture provides
382 the most substantial benefits in terms of prediction accuracy and consistency.

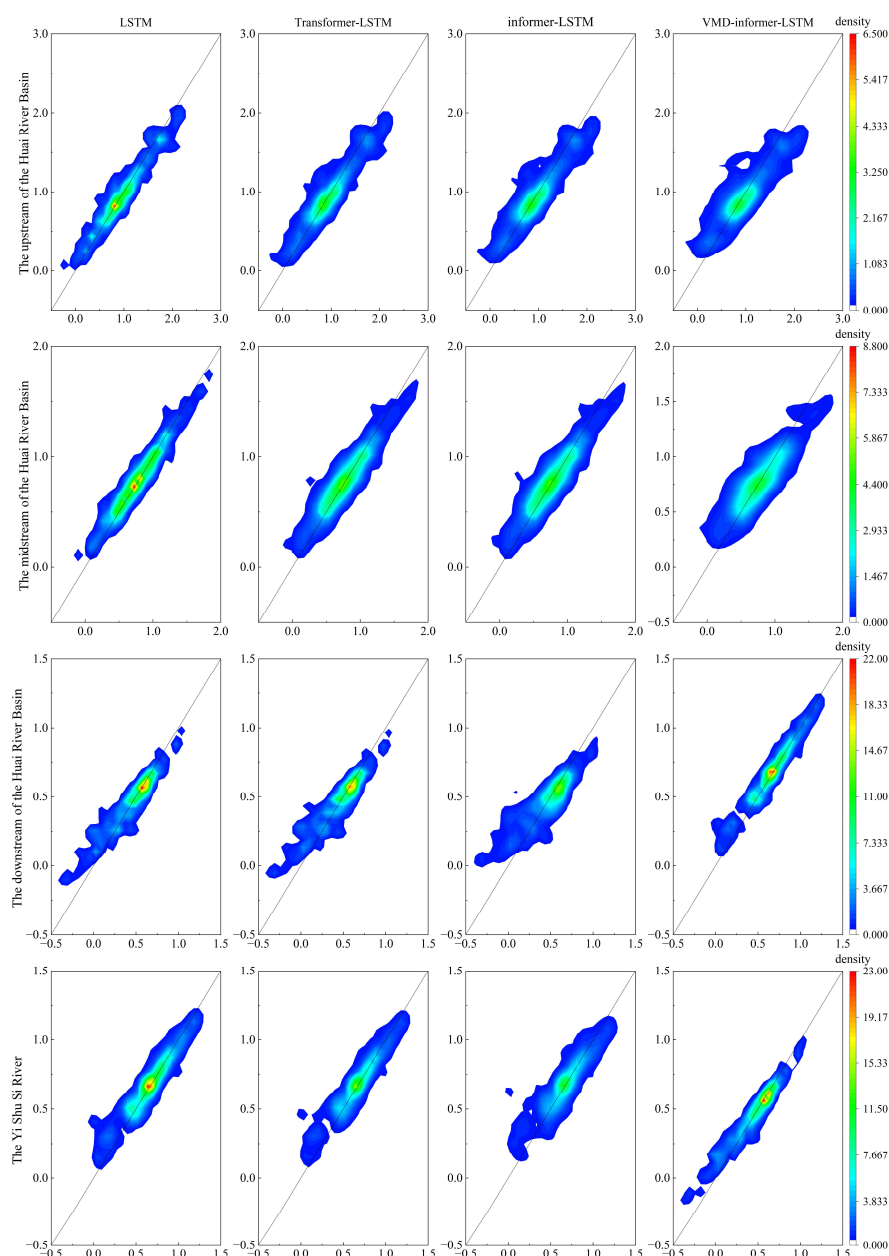
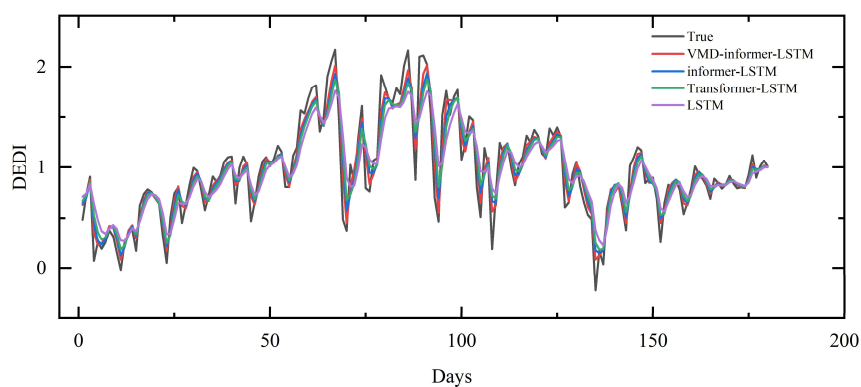
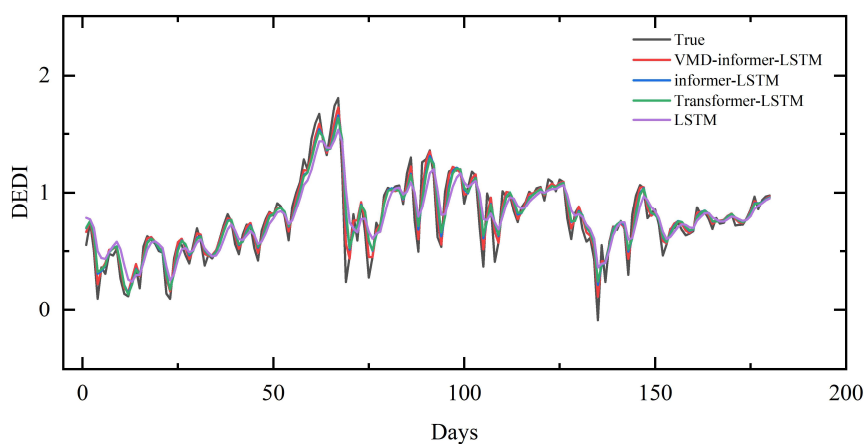


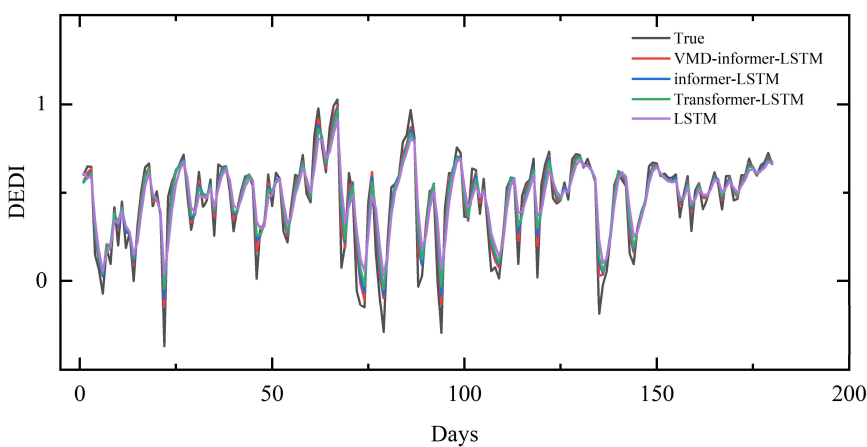
Figure 7 Evaluation indicators of different regions within the Huaihe River Basin



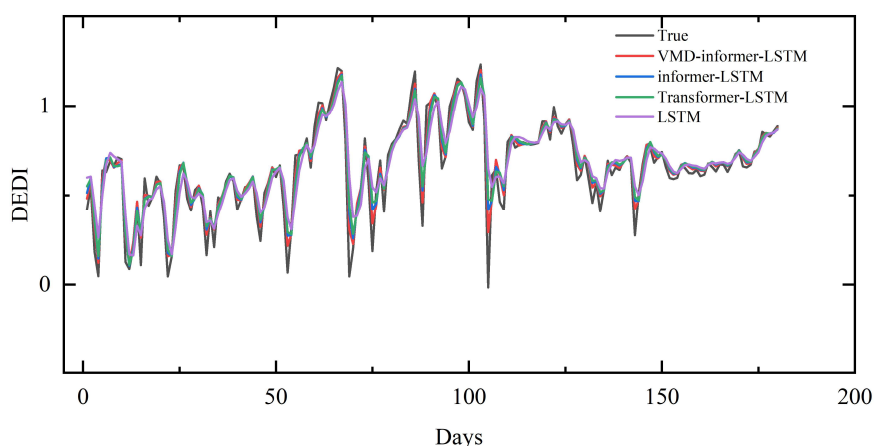
(a)



(b)



(c)



(d)

Figure 8 Line charts of different models' 180 - day predictions in four Huaihe River Basin Regions: (a) Upstream; (b) Midstream; (c) Downstream; (d) Yi Shu Si River

Fig. 7 and Fig. 8 show scatter plots and line charts of different models' 180-day predictions in different Huaihe River Basin regions. As illustrated in Fig. 7, LSTM yields the lowest R^2 values (0.76–0.78) across all subplots and is therefore the poorest performer; its scatter points visibly diverge from the 1:1 line, reflecting the largest prediction errors. Although informer-LSTM is less accurate than VMD-informer-LSTM, it maintains a stable R^2 of about 0.89, and the scatter deviation is markedly smaller than those of Transformer-LSTM and LSTM.

Fig. 8 further indicates that all four models successfully capture the overall drought trend, yet differ in precision. When the line plots are examined in conjunction, it becomes clear that VMD-informer-LSTM outperforms the other three models, delivering superior agreement between simulated and observed values, higher prediction accuracy, and the best overall performance. informer-LSTM and Transformer-LSTM rank next, whereas LSTM only roughly reproduces the drought trend and performs poorly at predicting extremes, resulting in the lowest predictive capability.

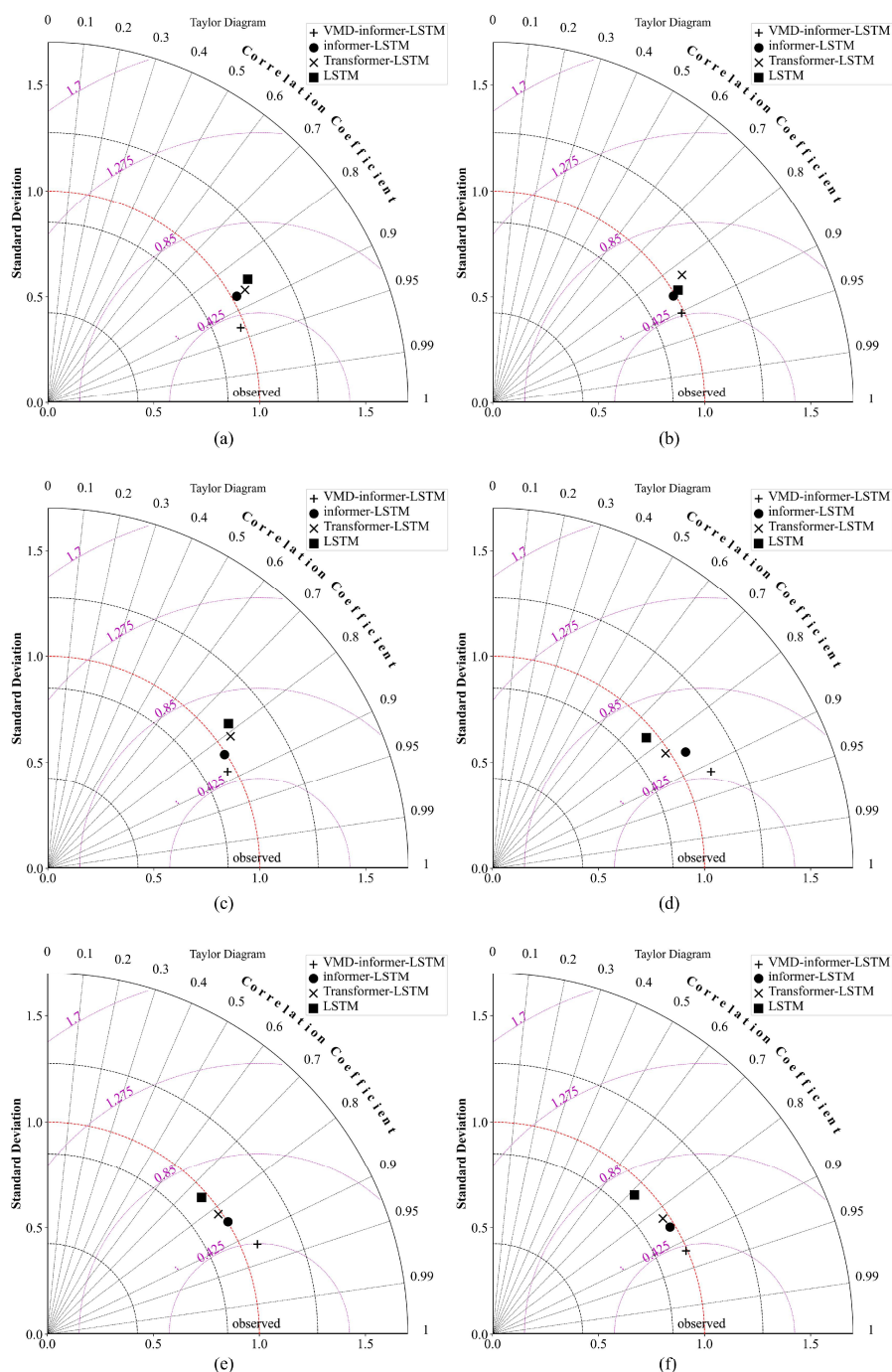


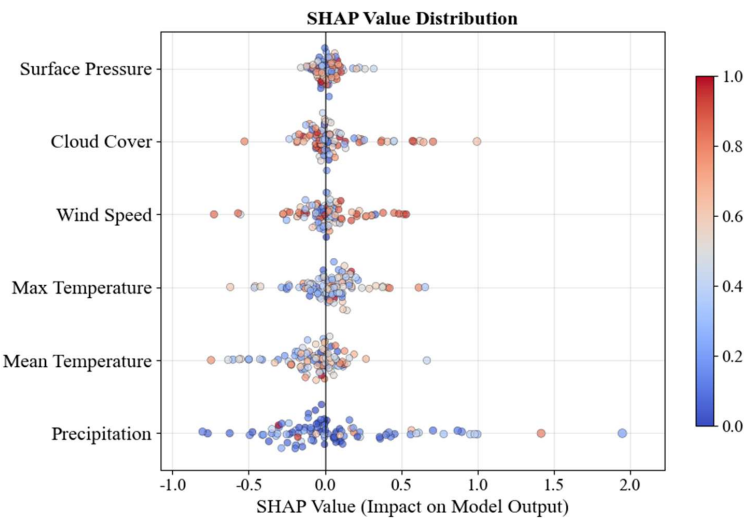
Figure 9 Taylor diagrams of different models across different lead times: (a) 7 days; (b) 15 days; (c) 30 days; (d) 60 days (e); 120 days; (f) 180 days



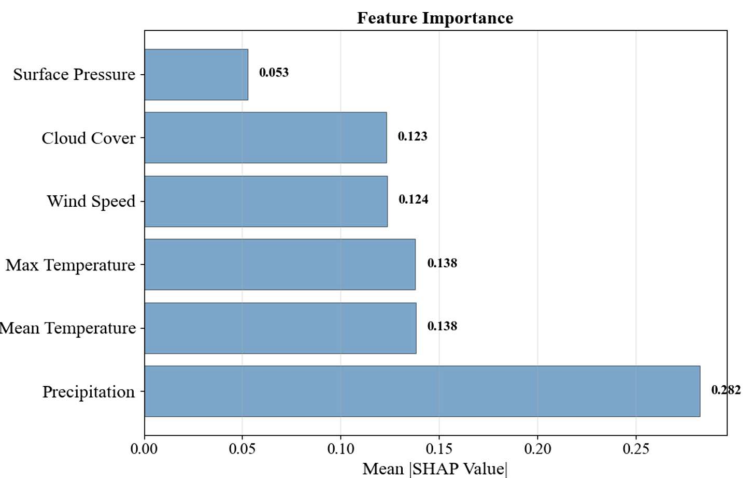
Fig. 9 presents Taylor diagrams that evaluate the predictive performance of various models across different lead times: (a) 7 days, (b) 15 days, (c) 30 days, (d) 60 days, (e) 120 days, and (f) 180 days. These diagrams provide a comprehensive assessment by integrating standard deviation and correlation coefficients from the observed data. The VMD-informer-LSTM model consistently shows superior predictive accuracy across all lead times, with its predictions closely aligned with the observed data, particularly in the upper, middle, and lower regions of the Huaihe River Basin and the Yi Shu Si River regions. At short lead times (7 and 15 days), all models perform relatively well, but the VMD-informer-LSTM model slightly outperforms the others. As the lead time extends to 30 and 60 days, the VMD-informer-LSTM model maintains high accuracy while other models show performance degradation, indicating a reduced ability to capture the underlying data patterns effectively. At long lead times (120 and 180 days), the VMD-informer-LSTM model's advantage becomes more pronounced, with its predictions remaining significantly closer to the observed data than other models, which exhibit more noticeable divergence. This suggests that the VMD-informer-LSTM model is better equipped to handle the increased uncertainty and complexity associated with long-term predictions, highlighting its robustness and reliability in predictive tasks, especially crucial in drought forecasting where lead time is a critical factor.

4.3 Model Influencing Factor Analysis

Fig. 10a presents a comprehensive SHAP value distribution analysis revealing the complex, non-linear relationships between meteorological variables and drought prediction outcomes. Precipitation emerges as the dominant predictor with predominantly positive SHAP contributions, indicating its critical role in alleviating drought conditions through direct water supply augmentation. However, the wide distribution of precipitation SHAP values (-1.00 to 2.00) suggests threshold-dependent effects, where low precipitation events contribute negatively to drought mitigation while high precipitation provides substantial positive contributions. Temperature exhibits a more complex influence pattern, with SHAP values distributed across both positive and negative domains, reflecting its dual role in drought dynamics: moderate temperatures may enhance vegetation water use efficiency (positive contribution), while extreme temperatures intensify evapotranspiration demands and soil moisture depletion (negative contribution). Fig. 10b quantifies that precipitation and mean temperature collectively account for approximately 49.00% of the total model decision-making process, with average SHAP magnitudes of 0.282 and 0.138 respectively. Surface pressure, cloud cover, and maximum temperature demonstrate moderate but consistent influences (SHAP magnitudes of 0.053 to 0.124), likely operating through indirect pathways affecting atmospheric moisture transport, radiation balance, and boundary layer dynamics. The concentrated distribution of these secondary variables' SHAP values suggests more linear, predictable relationships with drought outcomes, contrasting with the high variability observed in precipitation and temperature effects, which reflects the non-stationary nature of hydro-climatic processes and the model's capacity to capture complex feature interactions across different drought severity conditions.



(a)



(b)

Figure 10 Relative contributions of meteorological variables to drought forecasting at a 180-day lead time

While this study demonstrates the superior performance of the VMD-informer-LSTM model through comprehensive comparative analysis, several aspects of model uncertainty warrant acknowledgement. The concentrated performance distributions observed in violin plots suggest relatively low model uncertainty across different geographical locations, with the VMD-informer-LSTM model showing the most stable performance (IQR: 0.05 for RMSE). However, systematic uncertainty quantification through techniques such as ensemble modeling, Monte Carlo dropout, or Bayesian approaches was not implemented in this study, representing a limitation that could be addressed in future research to provide confidence intervals for predictions and better understand prediction reliability under different hydroclimatic conditions.



463 The spatial analysis reveals that prediction accuracy varies across the basin, with slightly
464 higher uncertainties observed along catchment peripheries. This is potentially related to boundary
465 effects or data quality variations. Future work should incorporate explicit uncertainty quantification
466 methods to enhance the model's operational applicability and provide decision-makers with
467 confidence measures alongside drought predictions.

468 4.4 Discussion

469 Fig. 11 illustrates the spatial prediction performance of the VMD-informer-LSTM model in the
470 Huaihe River Basin. Overall, the model achieves the highest accuracy in the first 90 days of
471 prediction, with an R^2 close to 0.92 and low error, effectively characterizing the evolution of drought.
472 As the prediction horizon extends beyond 90 days, the accuracy shows a noticeable decline,
473 reflecting the increasing difficulty of capturing long-term drought dynamics. In terms of spatial
474 distribution, the upstream area performs the best, accurately reproducing the observed drought
475 process. The downstream area follows, with the overall drought trend being tracked, though there
476 is a tendency of underestimation in drought intensity. The midstream area shows slightly larger
477 errors, but maintains high consistency with observations on a long-term scale. The Yi Shu Si River
478 region shows a relatively balanced performance, with the model effectively reflecting changes in
479 drought levels.

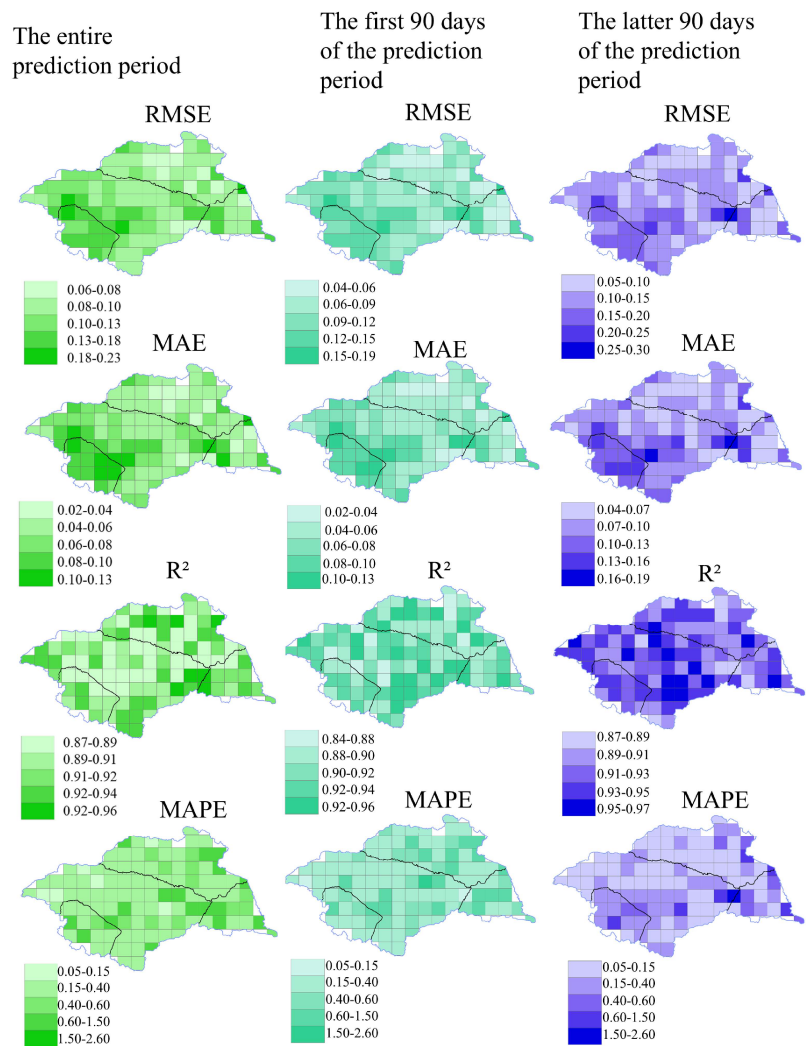


Figure 11 The spatial distribution of VMD-informer-LSTM Model performance

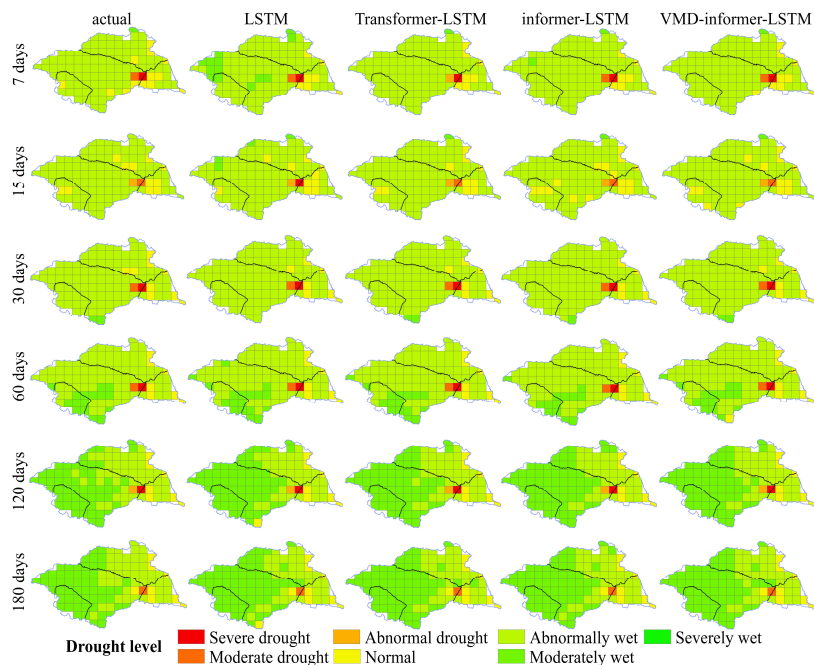


Figure 12 Comparison of drought forecasting model performance at different time scales

Fig. 12 further reveals the characteristics of drought category distribution under different prediction horizons and reflects regional differences. In the short-term predictions (first 15 days), although some models exhibit prediction errors, the overall results in the upstream, midstream, downstream, and Yi Shu Si River regions remain broadly consistent with observations. At the 7-day horizon, the LSTM misclassifies 11 grid cells, identifying the abnormally wet category as moderately wet. At 15 days, the informer-LSTM shows errors in 4 grid cells, misclassifying abnormally wet conditions as normal.

In the medium-term predictions (30–60 days), the VMD-informer-LSTM demonstrates the best performance, with only 2 misclassified grid cells at both horizons, whereas the other three models show larger deviations, mainly concentrated in the upstream, midstream, and Yi Shu Si River regions. In the long-term predictions (120–180 days), prediction errors increase across all models; however, the VMD-informer-LSTM continues to maintain the highest overall accuracy. Across all prediction periods, models exhibit a common tendency to underestimate drought categories, with the VMD-informer-LSTM showing the smallest degree of underestimation.

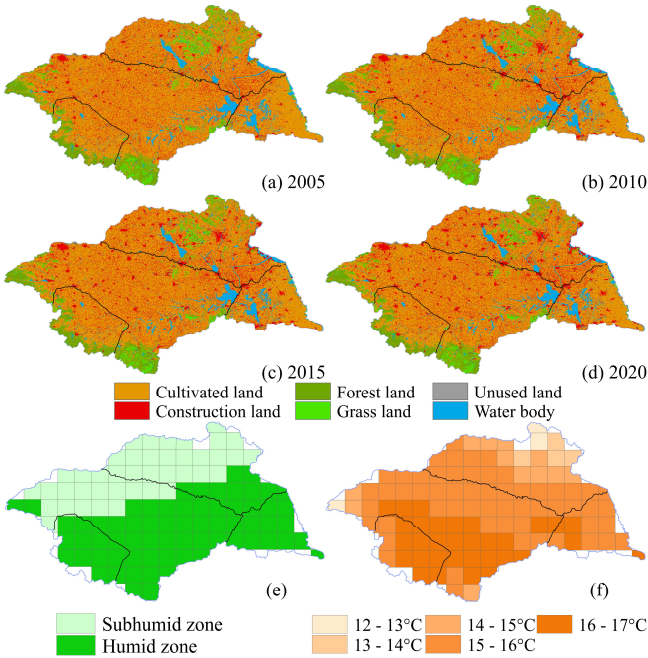
Overall, it can be seen that the upstream and downstream regions achieved the highest observations consistency, followed by the Yi Shu Si River region, while the midstream region performed the weakest.



501

Table 2 Area of land use types in Huaihe River basin from 2005 to 2020(km²)

Year	Cultivated Land	Forest land	Grassland	Water Body	Building	Unused Land
2005	187254	16550	10149	13159	34739	213
2010	186078	16593	10117	13224	35841	212
2015	184597	16539	10049	13326	37326	231
2020	180161	16052	8083	14282	42801	168



502

503

504

505

506

507

508

509

510

511

512

513

514

515

516

517

518

519

520

Figure 13 Distribution of Land Use, Climate Zones, and Multi-year Average Temperature in the Huaihe River Basin (a)–(d) Spatiotemporal distribution of land use in the Huaihe River Basin from 2005 to 2020; (e) Distribution map of semi-humid and humid zones in the Huaihe River Basin; (f) Distribution map of multi-year average temperature in the Huaihe River Basin

Further combining Table 2 and Fig. 13 provides a clearer understanding of the reasons for the differences in model prediction accuracy across different regions. From 2005 to 2020, the cultivated land in the basin continuously decreased (from 187,254 km² to 180,161 km²), the construction land significantly increased (from 34,739 km² to 42,801 km²), the grassland area markedly declined, and the water area slightly increased. In the midstream region, the reduction of cultivated land, forest land, and grassland, coupled with the increase in construction land leading to the expansion of impervious surfaces, has altered the water cycle process. This has caused the model's prediction to underestimate drought severity, demonstrating that environmental changes have exacerbated hydrological droughts.

Meanwhile, Figure 13 shows distinct climatic zone characteristics: the upstream, southern midstream, downstream, and southern regions of the Yi Shu Si River are in the humid zone, where the annual mean temperature in the upstream and its adjacent southern midstream regions is close to 17°C, and the annual mean temperature in the downstream and its adjacent southern midstream regions as well as the southern regions of the Yi Shu Si River is between 13–16°C. In contrast, the



northern midstream and northern regions of the Yi Shu Si River are in the semi-humid zone, with an annual mean temperature between 12°C and 15°C. Overall, the prediction results of several models underestimated hydrological drought, with misclassifications mainly concentrated in the transition zones between the humid and semi-humid regions. The semi-humid regions showed relatively more frequent errors compared to the humid regions.

The results indicate that the VMD-informer-LSTM model demonstrates relatively high prediction accuracy within the initial 30 – 90 days in the temporal dimension, while the accuracy shows a slight decrease during the 120 – 180 days phase. In the spatial dimension, the upstream and downstream regions show the highest consistency between prediction results and observations. This is followed by the Yi Shu Si River region, with the midstream region being the weakest.

5. Conclusion

This study takes the Huaihe River Basin in China as an example and constructs the VMD-informer-LSTM model, and compares it with the LSTM, Transformer-LSTM, and informer-LSTM models to verify its ability to predict hydrological drought in both temporal and spatial dimensions, and influencing factors are quantitatively analyzed. The main conclusions are as follows:

(1) The VMD-informer-LSTM model shows clear advantages in drought forecasting across different lead times and drought severity levels. Compared with the baseline LSTM, it improves R^2 by 28.4% ($0.7156 \rightarrow 0.9191$) and reduces RMSE by 46.2% ($0.2087 \rightarrow 0.1122$). Further comparisons reveal that the single LSTM struggles to capture the complex drought process and performs the poorest in all models' predictions. Transformer-LSTM improves accuracy to some extent, but there is still significant error accumulation in long-term predictions. The informer-LSTM, leveraging the sparse self-attention mechanism and generative decoding approach of the informer, can balance efficiency and accuracy in long time series prediction, showing greater stability than Transformer-LSTM and being the best among the three benchmark models. However, the VMD-informer-LSTM, by introducing VMD decomposition to further extract multi-scale features and combining the long sequence modeling advantages of the informer with the local dynamic characterization ability of LSTM, achieves multi-level information fusion. Therefore, the VMD-informer-LSTM model achieves the highest precision in short-term forecasting (7 days), has the smallest error growth rate in the medium term (30–60 days), and can still more effectively characterize the evolution of drought in the long term (120–180 days). Its underestimation of drought intensity is significantly lower than other models.

(2) The spatial prediction performance of the VMD informant LSTM model is influenced by land use and climate regions. Within the entire watershed, all models showed excellent prediction performance within a 30 day prediction period, with the VMD-informer-LSTM model being the most accurate. However, within a prediction period of 120–180 days, the prediction accuracy of all models significantly decreased throughout the watershed. Overall, the predicted drought intensity was relatively mild, with misclassifications mainly concentrated in the transition zones between the humid and semi-humid regions, and errors occurring more frequently in the semi-humid regions compared to the humid regions. The model performs best in the upstream region, followed by the downstream and Yishu River regions, while prediction accuracy in the midstream region is relatively weak. With the extension of the forecast lead time, this downward trend is most evident in the middle reaches, where the reduction of arable land, grassland, and forest land, as well as the expansion of construction land, have changed the water cycle process, indicating that human



564 activities have exacerbated drought.

565 (3) The SHAP analysis enhances the interpretability of the VMD-informer-LSTM model by
 566 revealing the relative importance of meteorological variables in drought prediction. Precipitation is
 567 the dominant factor, contributing about 28.2% to model decisions, followed by mean temperature
 568 (13.8%), while surface pressure, cloud cover, and maximum temperature together account for about
 569 15–20%. These results confirm that the model effectively identifies key meteorological drivers and
 570 enhances the interpretability of drought forecasting.

571 Author Contributions:

572 Conceptualization: Min Li, Ming Ou, Yuhang Yao, Changman Yin
 573 Data curation: Ming Ou
 574 Formal analysis: Min Li, Ming Ou
 575 Funding acquisition: Min Li
 576 Investigation: Min Li, Ming Ou
 577 Methodology: Min Li, Ming Ou
 578 Software: Min Li
 579 Supervision: Ming Ou, Yuhang Yao, Changman Yin
 580 Validation: Min Li
 581 Visualization: Ming Ou, Yuhang Yao, Changman Yin
 582 Writing – original draft: Min Li, Ming Ou
 583 Writing – review & editing: Yuhang Yao, Changman Yin

584 Declaration of competing interest

585 The authors declare no conflicts of interest relevant to this study.

586 Data Availability Statement

587 The gridded daily precipitation, evaporation, potential evaporation, mean temperature,
 588 maximum temperature, cloud cover, surface pressure, and wind speed data with a spatial r
 589 esolution of 0.25° were obtained from ERA5 post-processed daily statistics on single level
 590 s from 1940 to present ([https://cds.climate.copernicus.eu/datasets/derived-era5-single-levels-da](https://cds.climate.copernicus.eu/datasets/derived-era5-single-levels-daily-statistics?tab=overview)
 591 [ily-statistics?tab=overview](https://cds.climate.copernicus.eu/datasets/derived-era5-single-levels-daily-statistics?tab=overview)), covering the period from January 1, 1984, to December 31, 20
 592 24. Concurrently, the land use data were sourced from the Chinese Academy of Sciences
 593 Resource and Environment Science Data Center (<https://www.resdc.cn/Default.aspx>). The co
 594 re implementation of the VMD–Informer–LSTM model used in this study is publicly avail
 595 able on GitHub at: <https://github.com/OUman648/vmd-informer-LSTM>.

596 Acknowledgements

597 This work was financially Supported by Open Research Fund Program of National Key
 598 Laboratory of Water Disaster Prevention, 2024490711, Natural Science Foundation of Jiangsu
 599 Province, BK20250906.

600 References

601 AghaKouchak, A., Farahmand, A., Melton, F. S., Teixeira, J., Anderson, M. C., Wardlow,
 602 B. D., & Hain, C. R. (2015). Remote sensing of drought: Progress, challenges and op



- 603 portunities. *Reviews of Geophysics*, 53(2), 452–480. <https://doi.org/10.1002/2014RG0004>
 604 56
- 605 Alsubih, M., Mallick, J., Talukdar, S., Salam, R., AlQadhi, S., Fattah, Md. A., & Thanh, N.
 606 V. (2021). An investigation of the short-term meteorological drought variability over Asir
 607 Region of Saudi Arabia. *Theoretical and Applied Climatology*, 145(1–2), 597–617. <https://doi.org/10.1007/s00704-021-03647-4>
 608 oi.org/10.1007/s00704-021-03647-4
- 609 Belayneh, A., Adamowski, J., Khalil, B., & Ozga-Zielinski, B. (2014). Long-term SPI droug
 610 ht forecasting in the Awash River Basin in Ethiopia using wavelet neural network and wa
 611 velet support vector regression models. *Journal of Hydrology*, 508, 418–429. <https://doi.org/10.1016/j.jhydrol.2013.10.052>
 612 10.1016/j.jhydrol.2013.10.052
- 613 Bengio, Y., Courville, A., & Vincent, P. (2013). Representation Learning: A Review and Ne
 614 w Perspectives. *IEEE Transactions on Pattern Analysis and Machine Intelligence*, 35(8), 1
 615 798–1828. <https://doi.org/10.1109/TPAMI.2013.50>
- 616 Box, G. E., Jenkins, G. M., Reinsel, G. C., & Ljung, G. M. (2015). *Time series analysis: F
 617 orecasting and control*. John Wiley & Sons.
- 618 Cook, B. I., Mankin, J. S., Marvel, K., Williams, A. P., Smerdon, J. E., & Anchukaitis, K.
 619 J. (2020). Twenty-First Century Drought Projections in the CMIP6 Forcing Scenarios. *Eart
 620 h's Future*, 8(6), e2019EF001461. <https://doi.org/10.1029/2019EF001461>
 620 h's Future, 8(6), e2019EF001461. <https://doi.org/10.1029/2019EF001461>
- 621 Dai, A. (2013). Increasing drought under global warming in observations and models. *Nature
 622 Climate Change*, 3(1), 52–58. <https://doi.org/10.1038/nclimate1633>
 622 Climate Change, 3(1), 52–58. <https://doi.org/10.1038/nclimate1633>
- 623 Dragomiretskiy, K., & Zosso, D. (2014). Variational Mode Decomposition. *IEEE Transactions
 624 on Signal Processing*, 62(3), 531–544. <https://doi.org/10.1109/TSP.2013.2288675>
 624 on Signal Processing, 62(3), 531–544. <https://doi.org/10.1109/TSP.2013.2288675>
- 625 Dutra, E., Wetterhall, F., Di Giuseppe, F., Naumann, G., Barbosa, P., Vogt, J., Pozzi, W., &
 626 Pappenberger, F. (2014). Global meteorological drought – Part 1: Probabilistic monitoring.
 627 *Hydrology and Earth System Sciences*, 18(7), 2657–2667. <https://doi.org/10.5194/hess-18-2657-2014>
 627 Hydrology and Earth System Sciences, 18(7), 2657–2667. <https://doi.org/10.5194/hess-18-2657-2014>
 628 7-2014
- 629 Ek, M. B., Mitchell, K. E., Lin, Y., Rogers, E., Grunmann, P., Koren, V., Gayno, G., & Tar
 630 pley, J. D. (2003). Implementation of Noah land surface model advances in the National
 631 Centers for Environmental Prediction operational mesoscale Eta model. *Journal of Geophys
 632 ical Research: Atmospheres*, 108(D22), 2002JD003296. <https://doi.org/10.1029/2002JD003296>
 632 ical Research: Atmospheres, 108(D22), 2002JD003296. <https://doi.org/10.1029/2002JD003296>
- 633 Gao, C., Zhang, Z., Zhai, J., Qing, L., & Mengting, Y. (2015). Research on meteorological t
 634 hresholds of drought and flood disaster: A case study in the Huai River Basin, China. *Sto
 635 chastic Environmental Research and Risk Assessment*, 29(1), 157–167. <https://doi.org/10.1007/s00477-014-0951-y>
 635 chastic Environmental Research and Risk Assessment, 29(1), 157–167. <https://doi.org/10.1007/s00477-014-0951-y>
 636 7/s00477-014-0951-y
- 637 Greff, K., Srivastava, R. K., Koutník, J., Steunebrink, B. R., & Schmidhuber, J. (2017). LST
 638 M: A Search Space Odyssey. *IEEE Transactions on Neural Networks and Learning System
 639 s*, 28(10), 2222–2232. <https://doi.org/10.1109/TNNLS.2016.2582924>
 639 s, 28(10), 2222–2232. <https://doi.org/10.1109/TNNLS.2016.2582924>
- 640 Hao, Z., Hao, F., Singh, V. P., Ouyang, W., & Cheng, H. (2017). An integrated package for
 641 drought monitoring, prediction and analysis to aid drought modeling and assessment. *Envir
 642 onmental Modelling & Software*, 91, 199–209. <https://doi.org/10.1016/j.envsoft.2017.02.008>
 642 onmental Modelling & Software, 91, 199–209. <https://doi.org/10.1016/j.envsoft.2017.02.008>
- 643 Hersbach, H., Bell, B., Berrisford, P., Hirahara, S., Horányi, A., Muñoz-Sabater, J., Nicolas,
 644 J., Peubey, C., Radu, R., Schepers, D., Simmons, A., Soci, C., Abdalla, S., Abellan, X., B
 645 alsamo, G., Bechtold, P., Biavati, G., Bidlot, J., Bonavita, M., ... Thépaut, J. (2020). The
 646 ERA5 global reanalysis. *Quarterly Journal of the Royal Meteorological Society*, 146(730),



- 1999–2049. <https://doi.org/10.1002/qj.3803>
- Hochreiter, S., & Schmidhuber, J. (1997). Long Short-Term Memory. *Neural Computation*, 9(8), 1735–1780. <https://doi.org/10.1162/neco.1997.9.8.1735>
- Huang, S., Huang, Q., Chang, J., Zhu, Y., Leng, G., & Xing, L. (2015). Drought structure based on a nonparametric multivariate standardized drought index across the Yellow River basin, China. *Journal of Hydrology*, 530, 127–136. <https://doi.org/10.1016/j.jhydrol.2015.09.042>
- Jacob, D., Petersen, J., Eggert, B., Alias, A., Christensen, O. B., Bouwer, L. M., Braun, A., Colette, A., Déqué, M., Georgievski, G., Georgopoulou, E., Gobiet, A., Menut, L., Nikulin, G., Haensler, A., Hempelmann, N., Jones, C., Keuler, K., Kovats, S., ... Yiou, P. (2014). EURO-CORDEX: New high-resolution climate change projections for European impact research. *Regional Environmental Change*, 14(2), 563–578. <https://doi.org/10.1007/s10113-013-0499-2>
- Jaseena, K. U., & Koor, B. C. (2022). Deterministic weather forecasting models based on intelligent predictors: A survey. *Journal of King Saud University - Computer and Information Sciences*, 34(6, Part B), 3393–3412. <https://doi.org/10.1016/j.jksuci.2020.09.009>
- Johnny, K., Pai, M. L., & S., A. (2022). A multivariate EMD-LSTM model aided with Time Dependent Intrinsic Cross-Correlation for monthly rainfall prediction. *Applied Soft Computing*, 123, 108941. <https://doi.org/10.1016/j.asoc.2022.108941>
- Kratzert, F., Klotz, D., Brenner, C., Schulz, K., & Herrnegger, M. (2018). Rainfall–runoff modelling using Long Short-Term Memory (LSTM) networks. *Hydrology and Earth System Sciences*, 22(11), 6005–6022. <https://doi.org/10.5194/hess-22-6005-2018>
- Lawrence, D. M., Oleson, K. W., Flanner, M. G., Thornton, P. E., Swenson, S. C., Lawrence, P. J., Zeng, X., Yang, Z.-L., Levis, S., Sakaguchi, K., Bonan, G. B., & Slater, A. G. (2011). Parameterization improvements and functional and structural advances in Version 4 of the Community Land Model: PARAMETERIZATION IMPROVEMENTS AND FUNCTIONAL AND STRUCTURAL ADVANCES. *Journal of Advances in Modeling Earth Systems*, 3(1), n/a–n/a. <https://doi.org/10.1029/2011MS00045>
- LeCun, Y., Bengio, Y., & Hinton, G. (2015). Deep learning. *Nature*, 521(7553), 436–444. <https://doi.org/10.1038/nature14539>
- Li, Z., Wu, H., Duan, S., Zhao, W., Ren, H., Liu, X., Leng, P., Tang, R., Ye, X., Zhu, J., Sun, Y., Si, M., Liu, M., Li, J., Zhang, X., Shang, G., Tang, B., Yan, G., & Zhou, C. (2023). Satellite Remote Sensing of Global Land Surface Temperature: Definition, Methods, Products, and Applications. *Reviews of Geophysics*, 61(1), e2022RG000777. <https://doi.org/10.1029/2022RG000777>
- Lundberg, S., & Lee, S.-I. (2017). *A Unified Approach to Interpreting Model Predictions* (Note. arXiv:1705.07874; Version 2). arXiv. <https://doi.org/10.48550/arXiv.1705.07874>
- Mishra, A. K., & Desai, V. R. (2005). Drought forecasting using stochastic models. *Stochastic Environmental Research and Risk Assessment*, 19(5), 326–339. <https://doi.org/10.1007/s00477-005-0238-4>
- Mo, K. C. (2008). Model-Based Drought Indices over the United States. *Journal of Hydrometeorology*, 9(6), 1212–1230. <https://doi.org/10.1175/2008JHM1002.1>
- Modarres, R. (2007). Streamflow drought time series forecasting. *Stochastic Environmental Research and Risk Assessment*, 21(3), 223–233. <https://doi.org/10.1007/s00477-006-0058-1>



- 691 Morid, S., Smakhtin, V., & Moghaddasi, M. (2006). Comparison of seven meteorological and
692 indices for drought monitoring in Iran. *International Journal of Climatology*, 26(7), 971–985.
693 <https://doi.org/10.1002/joc.1264>
- 694 Mosavi, A., Ozturk, P., & Chau, K. (2018). Flood Prediction Using Machine Learning Models:
695 A Literature Review. *Water*, 10(11), 1536. <https://doi.org/10.3390/w10111536>
- 696 Mossad, A., & Alazba, A. (2015). Drought Forecasting Using Stochastic Models in a Hyper-
697 Arid Climate. *Atmosphere*, 6(4), 410–430. <https://doi.org/10.3390/atmos6040410>
- 698 Muñoz-Sabater, J., Dutra, E., Agustí-Panareda, A., Albergel, C., Arduini, G., Balsamo, G., Boussetta,
699 S., Choulga, M., Harrigan, S., Hersbach, H., Martens, B., Miralles, D. G., Piles, M., Rodríguez-Fernández,
700 N. J., Zsoter, E., Buontempo, C., & Thépaut, J.-N. (2021). ERA5-Land: A state-of-the-art global reanalysis dataset for land applications. *Earth System Science Data*, 13(9), 4349–4383. <https://doi.org/10.5194/essd-13-4349-2021>
- 701 Myttenaere, A. D., Golden, B., Grand, B. L., & Rossi, F. (2016). Mean Absolute Percentage
702 Error for regression models. *Neurocomputing*, 192, 38–48. <https://doi.org/10.1016/j.neucom.2015.12.114>
- 703 Nash, J. E., & Sutcliffe, J. V. (1970). River flow forecasting through conceptual models part
704 I—A discussion of principles. *Journal of Hydrology*, 10(3), 282–290.
- 705 Pozzi, W., Sheffield, J., Stefanski, R., Cripe, D., Pulwarty, R., Vogt, J. V., Heim, R. R., Brewer, M. J., Svoboda, M., Westerhoff, R., Van Dijk, A. I. J. M., Lloyd-Hughes, B., Pappenberger, F., Werner, M., Dutra, E., Wetterhall, F., Wagner, W., Schubert, S., Mo, K., ... Lawford, R. (2013). Toward Global Drought Early Warning Capability: Expanding International Cooperation for the Development of a Framework for Monitoring and Forecasting. *Bulletin of the American Meteorological Society*, 94(6), 776–785. <https://doi.org/10.1175/BAMS-D-11-00176.1>
- 715 Rummukainen, M. (2010). State-of-the-art with regional climate models. *WIREs Climate Change*, 1(1), 82–96. <https://doi.org/10.1002/wcc.8>
- 716 Saha, S., Moorthi, S., Wu, X., Wang, J., Nadiga, S., Tripp, P., Behringer, D., Hou, Y.-T., Chouhan, H., Iredell, M., Ek, M., Meng, J., Yang, R., Mendez, M. P., Van Den Dool, H., Zhang, Q., Wang, W., Chen, M., & Becker, E. (2014). The NCEP Climate Forecast System Version 2. *Journal of Climate*, 27(6), 2185–2208. <https://doi.org/10.1175/JCLI-D-12-00823.1>
- 721 Schmidhuber, J. (2015). Deep learning in neural networks: An overview. *Neural Networks*, 61, 85–117. <https://doi.org/10.1016/j.neunet.2014.09.003>
- 722 Shlezinger, N., Whang, J., Eldar, Y. C., & Dimakis, A. G. (2023). Model-Based Deep Learning. *Proceedings of the IEEE*, 111(5), 465–499. <https://doi.org/10.1109/JPROC.2023.3247480>
- 723 Sit, M., Demiray, B. Z., Xiang, Z., Ewing, G. J., Sermet, Y., & Demir, I. (2020). A comprehensive review of deep learning applications in hydrology and water resources. *Water Science and Technology*, 82(12), 2635–2670. <https://doi.org/10.2166/wst.2020.369>
- 724 Svoboda, M., LeCompte, D., Hayes, M., Heim, R., Gleason, K., Angel, J., Rippey, B., Tinker, R., Palecki, M., Stooksbury, D., Miskus, D., & Stephens, S. (2002). THE DROUGHT MONITOR. *Bulletin of the American Meteorological Society*, 83(8), 1181–1190. <https://doi.org/10.1175/1520-0477-83.8.1181>
- 729 Trenberth, K. E., Dai, A., Van Der Schrier, G., Jones, P. D., Barichivich, J., Briffa, K. R., & Sheffield, J. (2014). Global warming and changes in drought. *Nature Climate Change*,



4(1), 17–22. <https://doi.org/10.1038/nclimate2067>

Vaswani, A., Shazeer, N., Parmar, N., Uszkoreit, J., Jones, L., Gomez, A. N., Kaiser, L., & Polosukhin, I. (2017). Attention is all you need. *Advances in Neural Information Processing Systems*, 30(1), 5998–6008.

Vicente-Serrano, S. M., Miralles, D. G., Domínguez-Castro, F., Azorin-Molina, C., El Kenawy, A., McVicar, T. R., Tomás-Burguera, M., Beguería, S., Maneta, M., & Peña-Gallardo, M. (2018). Global Assessment of the Standardized Evapotranspiration Deficit Index (SEDI) for Drought Analysis and Monitoring. *Journal of Climate*, 31(14), 5371–5393. <https://doi.org/10.1175/JCLI-D-17-0775.1>

Wang, H., Liang, Q., Hancock, J. T., & Khoshgoftaar, T. M. (2024). Feature selection strategies: A comparative analysis of SHAP-value and importance-based methods. *Journal of Big Data*, 11(1), 44. <https://doi.org/10.1186/s40537-024-00905-w>

Willmott, C., & Matsuura, K. (2005). Advantages of the mean absolute error (MAE) over the root mean square error (RMSE) in assessing average model performance. *Climate Research*, 30, 79–82. <https://doi.org/10.3354/cr030079>

Wood, A. W., Hopson, T., Newman, A., Brekke, L., Arnold, J., & Clark, M. (2016). Quantifying Streamflow Forecast Skill Elasticity to Initial Condition and Climate Prediction Skill. *Journal of Hydrometeorology*, 17(2), 651–668. <https://doi.org/10.1175/JHM-D-14-0213.1>

Yao, T., Zhao, Q., Wu, C., Hu, X., Xia, C., Wang, X., Sang, G., Liu, J., & Wang, H. (2024). Spatio-temporal Variation Characteristics of Extreme Climate Events and Their Teleconnections to Large-scale Ocean-atmospheric Circulation Patterns in Huaihe River Basin, China During 1959–2019. *Chinese Geographical Science*, 34(1), 118–134. <https://doi.org/10.1007/s11769-023-1398-1>

Yuan, S., & Quiring, S. M. (2017). Evaluation of soil moisture in CMIP5 simulations over the contiguous United States using in situ and satellite observations. *Hydrology and Earth System Sciences*, 21(4), 2203–2218. <https://doi.org/10.5194/hess-21-2203-2017>

Zhang, J., Xin, X., Shang, Y., Wang, Y., & Zhang, L. (2023). Nonstationary significant wave height forecasting with a hybrid VMD-CNN model. *Ocean Engineering*, 285, 115338. <https://doi.org/10.1016/j.oceaneng.2023.115338>

Zhang, L., Lin, J., Liu, B., Zhang, Z., Yan, X., & Wei, M. (2019). A Review on Deep Learning Applications in Prognostics and Health Management. *IEEE Access*, 7, 162415–162438. <https://doi.org/10.1109/ACCESS.2019.2950985>

Zhang, Q., Kong, D., Shi, P., Singh, V. P., & Sun, P. (2018). Vegetation phenology on the Qinghai-Tibetan Plateau and its response to climate change (1982–2013). *Agricultural and Forest Meteorology*, 248, 408–417. <https://doi.org/10.1016/j.agrformet.2017.10.026>

Zhang, Q., Zhang, J., Yan, D., & Wang, Y. (2014). Extreme precipitation events identified using detrended fluctuation analysis (DFA) in Anhui, China. *Theoretical and Applied Climatology*, 117(1–2), 169–174. <https://doi.org/10.1007/s00704-013-0986-x>

Zhang, X., Duan, Y., Duan, J., Jian, D., & Ma, Z. (2022). A daily drought index based on evapotranspiration and its application in regional drought analyses. *Science China Earth Sciences*, 65(2), 317–336. <https://doi.org/10.1007/s11430-021-9822-y>

Zhao, L., Li, Z., Qu, L., Zhang, J., & Teng, B. (2023). A hybrid VMD-LSTM/GRU model to predict non-stationary and irregular waves on the east coast of China. *Ocean Engineering*, 276, 114136. <https://doi.org/10.1016/j.oceaneng.2023.114136>



779 Zhou, H., Zhang, S., Peng, J., Zhang, S., Li, J., Xiong, H., & Zhang, W. (2021a). informer:
780 Beyond Efficient Transformer for Long Sequence Time-Series Forecasting. *Proceedings of*
781 *the AAAI Conference on Artificial Intelligence*, 35(12), 11106–11115. [https://doi.org/10.1609/](https://doi.org/10.1609/aaai.v35i12.17325)
782 [aaai.v35i12.17325](https://doi.org/10.1609/aaai.v35i12.17325)
783 Zhou, H., Zhang, S., Peng, J., Zhang, S., Li, J., Xiong, H., & Zhang, W. (2021b). informer:
784 Beyond Efficient Transformer for Long Sequence Time-Series Forecasting. *Proceedings of*
785 *the AAAI Conference on Artificial Intelligence*, 35(12), 11106–11115. [https://doi.org/10.1609/](https://doi.org/10.1609/aaai.v35i12.17325)
786 [aaai.v35i12.17325](https://doi.org/10.1609/aaai.v35i12.17325)
787 Zuo, G., Luo, J., Wang, N., Lian, Y., & He, X. (2020). Decomposition ensemble model bas
788 ed on variational mode decomposition and long short-term memory for streamflow forecast
789 ing. *Journal of Hydrology*, 585, 124776. <https://doi.org/10.1016/j.jhydrol.2020.124776>
790